Combined immunodeficiency and hypoglycemia associated with mutations in hypoxia upregulated 1

To the Editor:

Immunodeficiencies featuring congenital neutropenia have varying presentations, including life-threatening bacterial infections. These conditions can be caused by defects in more than 10 genes.[1-3] Most genes operate in the endolysosomal system, and their perturbed action induces unfolded protein response and altered mitochondrial function. The resulting cell stress drives neutrophils to apoptosis.[1-3]

We evaluated a 45-year-old woman showing symptoms of combined immunodeficiency and disturbed glucose metabolism since birth (for detailed case description, see this article's Online Repository at www.jacionline.org). She was born small for gestational age and her subsequent growth was poor. Her appearance was slightly dysmorphic, featuring oval face, pectus carinatum, and broad long bone metaphyses. During childhood, she experienced episodes of stress-induced hypoglycemia. From infancy to adulthood, she suffered from numerous septic infections of the respiratory tract, skin, and mucous membranes. At age 4 years, she had severe septic herpetic gingivostomatitis, after which herpetic stomatitis recurred monthly for several years. In adulthood, she contracted herpetic encephalitis followed by recurring condylomatous warts in her thighs and genital area. G-CSF and intravenous immunoglobulin treatment were initiated in her 20s, which led to the normalization of her absolute neutrophil count and significantly decreased the rate of bacterial infections. An immunodysregulatory component was evident, as the patient developed hidradenitis suppurativa in her teens and relapsing Takayasu arteritis as an adult. Currently, the patient receives G-CSF, immunoglobulin replacement therapy, rituximab, and oral prednisolone (5 mg/d).

Detailed immunological workup is presented in Tables E1-E3 in this article's Online Repository at www.jacionline.org. The patient showed broad abnormalities in the myeloid lineage. She had microcytic anemia, fluctuating thrombocytopenia, and constant granulocytopenia (see Table E1 in this article's Online Repository at www.jacionline.org). Neutrophils showed poor chemotaxis and increased activation. Bone marrow biopsies showed inconstant myeloid maturation arrest that resolved on G-GSF treatment (data not shown).

In addition, antigen presentation and adaptive immunity were affected. Both plasmacytoid and monocytoid dendritic cells were reduced in peripheral blood, and the expression of costimulatory CD86 molecule was low in both monocytoid dendritic cells and monocytes. These together with a low PHA stimulation response suggested impaired antigen presentation. In the T-cell compartment, the proportions of $CD4^+$ and $CD8^+$ T cells were within normal range, with naive $CCR7^+CD45RA^+$ cells dominating the repertoire. The B- cell count was very low, and B-cell development skewed toward mature B cells with reduced switched memory B cells. Despite normal immunoglobulin levels, responses to polysaccharide antigens were completely absent. It is unlikely that the observed changes are due to the patient's immunosuppressive regimen because most studies were carried either without or with low-dose immunosuppression (prednisolone 5 mg/d).

Because of a suspected novel primary immunodeficiency, we performed whole-exome sequencing. We identified novel compound heterozygous missense mutations in the hypoxia upregulated 1 (*HYOU1*) gene (Fig 1, *A*; also see Fig E1 in this article's Online Repository at www.jacionline.org).[4,5] The mutations (chr11: 118922614 C>G, p.A419P and chr11:118924936 A>G, p.Y231H) localized to the ATPase domain of HYOU1, negatively affecting conserved residues. HYOU1 is a chaperone that localizes to endoplasmic reticulum (ER) and mitochondria, and participates in cell stress responses, including oxidative stress and unfolded protein response.[4,6,7] Because most genes that cause congenital neutropenia perform similar functions, HYOU1 was considered a good candidate (for detailed comparison, see Table E4 in this article's Online Repository at www.jacionline.org). HYOU1 further belongs to herpes infection-induced proteome.[8]

We hypothesized that mutations in HYOU1 ATPase domain would impair ATP hydrolysis, thereby hampering the conformational changes required for HYOU1 chaperone function.[4,5] Consequently, this could lead to altered substrate binding. To test this, we performed affinity-purification mass spectrometry (AP-MS) on Strep-tagged wild type (WT) and mutant (MT) HYOU1 proteins expressed in tetracycline-inducible HEK293 cell lines. Both mutants bound with high affinity to a range of proteins that did not bind to WT HYOU1 (Fig 1, *C*). Thus, the binding profiles of the mutated HYOU1 proteins seemed altered, leading to ectopic protein binding.

To measure ER stress, we performed RNA sequencing on patient and control primary skin fibroblasts with and without tunicamycin, a compound that induces unfolded protein response (Fig 1, *B*; see Fig E2 in this article's Online Repository at www.jacionline.org). Compared with normal controls, the transcriptional profile was strikingly different in patient cells, and transcripts from ectopic Y231H and A419P interaction partners were upregulated. In steady state, the transcriptome suggested enhanced protein synthesis, glucose metabolism, and redox enzyme transcription in patient cells. Interestingly, a clear enrichment in redox proteins was also noted among HYOU1-binding partners in AP-MS (Fig 1, *C*).

As results from RNA sequencing and AP-MS pointed to altered cell metabolism, we performed mass spectrometry–based targeted analysis of 100 metabolites in patient and control fibroblasts (see Fig E3 in this article's Online Repository at www.jacionline.org). Again, we noted altered quantities of metabolites in pathways participating in redox balance.

To further characterize the phenotype, we studied patient and healthy control neutrophils with electron microscopy. The ER morphology was normal. However, we noted increased numbers of mitochondria along with high reactive oxygen species production in patient neutrophils (Fig 1, *D* and E, and see Table E1). To see whether the increased mitochondrial quantity and altered redox balance were caused by defective mitochondrial respiration, we performed XF Cell Mito Stress test on patient and healthy control fibroblasts (see Fig E3 in this article's Online Repository at www.jacionline.org). The patient fibroblasts performed consistently on low normal scale; significant alterations, however, were not evident.

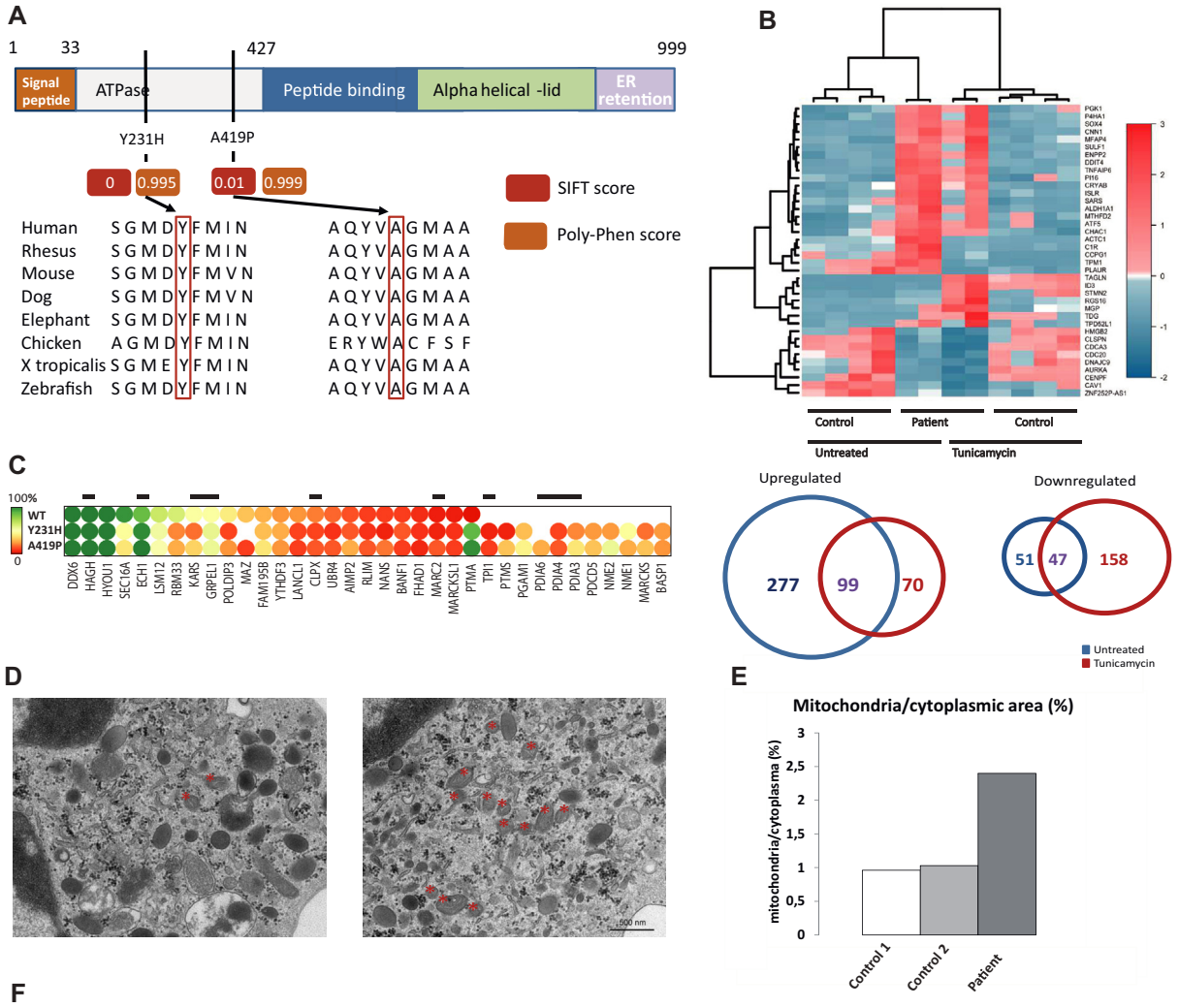

F

Pathway	RNA-seq	Binding assay	Metabolic assay
Redox	Redox balance ($p<10^{-5}$)	Intramolecular oxidoreductase activity ($p<10^{-4}$)	Glutathione metabolism ($p<0.001$) Cysteine metabolism ($p<0.005$)
Protein synthesis	Protein biosynthesis ($p<10^{-15}$)	Protein folding ($p<0.05$)	RNA transcription ($p=0.005$)
	Ribosome ($p<10^{-8}$)		Protein biosynthesis ($p<0.05$)
Glucose metabolism	Glucose metabolism ($p<10^{-6}$)	Glycolysis ($p=0.08$)	Glucose-alanine cycle ($p<0.05$)

FIG 1. A, HYOU1 structure[4] with the observed mutations. **B,** RNA expression profile in primary fibroblasts. **C,** Interaction partners of WT and mutant HYOU1 proteins as determined by affinity-purification mass-spectrometry (AP-MS). Black line denotes mitochondrial proteins. **D** and **E,** Electron micrograph figures of control (left) and patient (right) neutrophils show abundant mitochondria. **F,** Comparison of enriched pathways between RNA sequencing, AP-MS (denoted as binding assay), and targeted metabolite profiling (referred as metabolic assay). *Poly-Phen*, Polymorphism Phenotyping (algorithm); *SIFT*, Sorting Intolerant from Tolerant (algorithm).

All these experiments suggested that the unfolded protein response and mitochondrial function were altered in the index case. The findings were consistent with previous knowledge on HYOU1 function, and strengthened the causative role of the mutations.

In conclusion, we describe a novel immunometabolic syndrome caused by recessive *HYOU1* mutations. The condition features hypoglycemia and severe bacterial and herpetic infections. Immunologically, granulocytopenia and B-cell and dendritic cell deficiency are evident. G-CSF treatment is effective in correcting neutropenia and with intravenous immunoglobulin reduces the rate of infections. Our results are in line with previous reports linking members of the endolysosomal system to congenital neutropenia, and suggest that perturbed redox balance plays a role in these conditions.

We sincerely thank the patient for her co-operation and patience. Ari Much and Timo Otonkoski are acknowledged for obtaining and performing skin fibroblast cultures, and Meri Kokkonen and Jatin Nandania for performing the metabolomics profiling. Personnel at Science for Life Laboratory Stockholm

are acknowledged for their expert technical assistance. The computations were performed on resources provided by SNIC through Uppsala Multidisciplinary Center for Advanced Computational Science (UPPMAX) under Project b201022 and b201069.

Emma M. Haapaniemi, MD[a,b,c]
Christopher L. Fogarty, MSc[b,d,e]
Salla Keskitalo, MSc[f]
Shintaro Katayama, PhD[a,g,h]
Helena Vihinen, DSc[i]
Mette Ilander, PhD[j,k]
Satu Mustjoki, MD[j,k]
Kaarel Krjutškov, PhD[a,g,l]
Markku Lehto, PhD[b,d,e]
Timo Hautala, MD[m]
Ove Eriksson, PhD[n]
Eija Jokitalo, PhD[i]
Vidya Velagapudi, PhD[o]
Markku Varjosalo, PhD[f]
Mikko Seppänen, MD[p]*
Juha Kere, MD[a,b,c,g]*

From [a]the Department of Biosciences and Nutrition, Karolinska Institutet, Huddinge, Sweden; [b]Folkhälsan Institute of Genetics, Folkhälsan Research Center, Helsinki, Finland; [c]the Research Programs Unit, Molecular Neurology, University of Helsinki, Helsinki, Finland; [d]Abdominal Center Nephrology, University of Helsinki and Helsinki University Hospital, Helsinki, Finland; [e]the Research Programs Unit, Diabetes and Obesity, University of Helsinki, Helsinki, Finland; [f]the Institute of Biotechnology, University of Helsinki, Helsinki, Finland; [g]the Center for Innovative Medicine, Karolinska Institutet, Huddinge, Sweden; [h]Science for Life Laboratory, Solna, Sweden; [i]the Institute of Biotechnology, Electron Microscopy Unit, University of Helsinki, Helsinki, Finland; [j]the Hematology Research Unit Helsinki, Helsinki University Hospital Comprehensive Cancer Center, Helsinki, Finland; [k]the Department of Clinical Chemistry, University of Helsinki, Helsinki, Finland; [l]Competence Centre on Health Technologies, Tartu, Estonia; [m]Oulu University Hospital, Oulu, Finland; [n]the Faculty of Medicine, Department of Biochemistry and Developmental Biology, University of Helsinki, Helsinki, Finland; [o]the Metabolomics Unit, Institute for Molecular Medicine Finland FIMM, University of Helsinki, Helsinki, Finland; [p]Rare Disease Center, Children's Hospital and Adult Immunodeficiency Unit, Inflammation Center, Helsinki University and Helsinki University Hospital, Helsinki, Finland. E-mail: emma.haapaniemi@ki.se.

*These authors contributed equally to this work.

The Academy of Finland, Finnish Medical Foundation, Sigrid Juselius Foundation, Karolinska Institutet Research Foundation, Swedish Research Council, and Strategic Research Programme in Diabetes supported this work.

Disclosure of potential conflict of interest: C. L. Fogarty has received board membership and is employed by Bug ID Oy and has received consultancy fees from Bain and Company. S. Mustjoki's institution has received a grant from Academy of Finland and Sigrid Juselius Foundation for the work under consideration; he has received consultancy fees from Novartis, BMS, and Pfizer for work outside of this work; his institution has received grants from Pfizer for other work; and he has received payment for lectures from Novartis, BMS, and Pfizer. T. Hautala has received honoraria from CSL Behring and Octapharma. M. Seppänen has received honoraria from Baxter, CSL Behring, Octapharma, and Sanquin. J. Kere's institution has received a grant as stated on the manuscript. The rest of the authors declare that they have no relevant conflicts of interest.

REFERENCES

1. Boztug K, Jarvinen PM, Salzer E, Racek T, Monch S, Garncarz W, et al. JAGN1 deficiency causes aberrant myeloid cell homeostasis and congenital neutropenia. Nat Genet 2014;46:1021-7.
2. Hauck F, Klein C. Pathogenic mechanisms and clinical implications of congenital neutropenia syndromes. Curr Opin Allergy Clin Immunol 2013; 13:596-606.
3. Vilboux T, Lev A, Malicdan MC, Simon AJ, Jarvinen P, Racek T, et al. A congenital neutrophil defect syndrome associated with mutations in VPS45. N Engl J Med 2013;369:54-65.
4. Takeuchi S. Molecular cloning, sequence, function and structural basis of human heart 150 kDa oxygen-regulated protein, an ER chaperone. Protein J 2006;25: 517-28.
5. Mayer MP, Bukau B. Hsp70 chaperones: cellular functions and molecular mechanism. Cell Mol Life Sci 2005;62:670-84.
6. Arrington DD, Schnellmann RG. Targeting of the molecular chaperone oxygen-regulated protein 150 (ORP150) to mitochondria and its induction by cellular stress. Am J Physiol Cell Physiol 2008;294:C641-50.
7. Ozawa K, Kuwabara K, Tamatani M, Takatsuji K, Tsukamoto Y, Kaneda S, et al. 150-kDa oxygen-regulated protein (ORP150) suppresses hypoxia-induced apoptotic cell death. J Biol Chem 1999;274:6397-404.
8. Berard AR, Coombs KM, Severini A. Quantification of the host response proteome after herpes simplex virus type 1 infection. J Proteome Res 2015;14:2121-42.

Available online November 29, 2016.
http://dx.doi.org/10.1016/j.jaci.2016.09.050

Peanut oral immunotherapy decreases IgE to Ara h 2 and Ara h 6 but does not enhance sensitization to cross-reactive allergens

To the Editor:

Oral immunotherapy (OIT) induces specific IgG_4 antibodies and regulatory T cells and leads to suppression of IgE-mediated reactions.[1] In pollen immunotherapy, specific IgE levels to pollen allergens decrease with increasing IgG_4.[2,3] We aimed to study whether peanut OIT would induce neosensitization or affect cross-reactive proteins by analyzing IgE sensitization profiles using microarrays. In addition, we analyzed IgG_4-IgE ratios to peanut allergens during OIT and assessed whether the cumulative protein dose ingested during treatment determines the changes in IgG_4/IgE.

Fifty-eight 6- to 18-year-old children and adolescents having moderate-to-severe peanut allergy participated in the study. The diagnosis was based on a double-blind placebo-controlled peanut challenge (n = 52) or serum IgE to Ara h 2 above 25 kU/L (27.8-365 kU/L) (n = 6). Thirty-nine patients received peanut OIT, whereas 19 patients continued to avoid peanuts. During 8 months, the daily peanut protein intake increased from 0.1 to 800 mg, after which patients ingested 4 peanuts daily. During the first 19 build-up weeks, the patients used roasted defatted peanut flour (Byrd Mill, Ashland, Va), which showed 100% allergen activity of Ara h 1, 2, 3, and 6, 30% of Ara h 8, but lack of (<20%) Ara h 9 activity in Immuno Solid-phase Allergen Chip (ImmunoCAP ISAC, Thermo Fisher Scientific, Uppsala, Sweden) inhibition assay.[4] From week 20 on, the patients consumed whole peanuts. Serum samples were drawn at baseline and after build-up.

We measured serum IgE to 112 allergen components using the ISAC with a detection limit of 0.3 ISAC standardized units for specific IgE (ISU-E). We measured IgE to hazelnut Cor a 14 and cashew Ana o 3, and IgE and IgG_4 to whole peanut extract, Ara h 1, 2, 3, 8, and 9, using ImmunoCAP (Thermo Fisher Scientific). IgE and IgG_4 to Ara h 6 were measured using an experimental ImmunoCAP test. Sensitization was defined as ≥0.3 ISU-E. The ethics committee at the Helsinki University Hospital approved the study protocol. Patients and 1 of their parents provided informed written consent. Data analysis protocols can be found in the Online Repository (available at www.jacionline.org).

At baseline, all 58 patients were sensitized to Ara h 2 (97%) and/or Ara h 6 (98%). In addition, the majority was sensitized to Ara h 1 (74%), Ara h 3 (70%), or Ara h 8 (79%), but only 9% were sensitized to Ara h 9. Sensitization to any Ara h 8–cross-reactive pathogenesis-related proteins group 10 (PR-10) protein occurred

CASE DESCRIPTION

The patient is a 41-year old woman born to nonconsanguineous parents after uneventful pregnancy. Family history is negative for major illnesses. She was born small for gestational age (2270 g/41 cm) at week 36+4. After birth, she developed hyperbilirubinemia and hypoglycemia, necessitating phototherapy and intravenous glucose administration. Some days later, she suffered from postpartum omphalitis caused by *Enterococcus faecalis* and was treated with intravenous antibiotics. Hypoglycemia, often precipitated by infection, recurred throughout childhood. Tested later, her insulin and glucagon levels were normal (10.5 mU/L and 164 ng/L, respectively); pediatric values were unavailable.

Her growth alternated between –2.5 and –3.2 SD, and end height became 152 cm (−2.9 SD) with an arm span of 154.5 cm. Her long bone metaphyses were abnormally broad on repeated X-ray examinations. Bone age was somewhat delayed until puberty. Although moderate learning problems were noted at school, her cognitive functions are normal. Her physical appearance is slightly dysmorphic, with somewhat narrow and oval face, high-sloped forehead, high hairline, low normal earlobes, broad nasal bridge, prominent narrow nose, micrognathia, high palate, mild pectus carinatum, and long slender fingers with narrow long nails. Her menarche was somewhat delayed (age 15 years).

At age 2 years, her thymus appeared hypoplastic in chest X-ray. After uncomplicated BCG vaccination, PPD test result became positive at 100 TU. Severe granulocytopenia with normal monocyte levels was noted at age 3 years, and antigranulocyte antibodies were negative. From early infancy to adulthood, she has suffered from numerous purulent infections in upper and lower respiratory tract, skin, and mucous membranes. These necessitated hospital admissions 5 to 6 times per year. The infections frequently became septic and required intravenous antibiotic treatment as well as repeated abscess drainages, tympanostomies, myringoplasties, and repetitive grommet placements, even in adulthood. Functional endoscopic sinus surgery was performed at age 28 years to alleviate purulent sinusitis. Common encapsulated pathogens (*S pneumoniae, S aureus, S pyogenes, S viridans*) were cultured from infections. At school age, she suffered from relapsing suppurative hidradenitis of the left axillar fossa that spontaneously disappeared in her late teens.

Recurrent aphthous stomatitis was diagnosed at an early age. At age 4 years, she also developed septic herpetic gingivostomatitis requiring intensive care. Herpetic stomatitis then recurred monthly for years. In adulthood, she suffered an episode of herpetic encephalitis. These subsequently lead to long-term valaciclovir prophylaxis. She was started on G-CSF and subcutaneous immunoglobulin replacement therapy in her 20s. These significantly decreased the rate of bacterial and viral infections.

In infancy and at preschool age, the patient also suffered from constant diarrhea and malabsorption, which later corrected spontaneously. No clear evidence for pancreatic insufficiency was noted; however, the level of serum amylase had repeatedly been below reference. Hepatomegaly with elevated alkaline phosphatase and activated partial thromboplastin time was first diagnosed at age 4 years after granulocyte transfusion during a septic episode and disappeared by the age of 9 years. At age 29 years, she again developed hepatomegaly with spontaneous resolution in subsequent years.

In her late 20s, she underwent several spontaneous miscarriages, mostly because of placental bleeding. Two of the pregnancies resulted in placental thrombosis and microabscesses, septic infection, and fetus mortus at week 20 to 22. Lupus anticoagulant and autoantibodies to phospholipase A2 receptor were positive.

At age 43 years, the patient developed acute high fever and chest pain. No signs of specific infections were found and she did not respond to broad-spectrum antibiotics. Based on computed tomography findings, Takayasu arteritis was diagnosed, with a favorable response to corticosteroid treatment. She has continued being active and is able to work despite frequent episodes of severe illnesses.

In addition to granulocytopenia and dendritic and B-cell deficiency, the patient has constant microcytic, hypochromic anemia (mean corpuscular volume 65) with normal serum iron indices. In addition, mild thrombocytopenia was present in childhood. As an adult, episodes of thrombocytopenia have been noted during infections. Bone marrow examinations occasionally but inconstantly showed both megakaryocytes with fragmented nucleoli and myeloid maturation arrest that resolved on G-CSF treatment. No signs of malignant transformation have been noted in repeated bone marrow examinations.

METHODS

Study participants

The study was conducted in accordance with principles of the Declaration of Helsinki and was approved by the Helsinki University Central Hospital Ethics Committee. Written informed consent was obtained from the patient and healthy controls.

DNA extraction and whole-exome sequencing

Genomic DNA was extracted from EDTA-blood samples or salivary samples using Qiagen FlexiGene DNA kit (Qiagen, Hilden, Germany) or OraGene DNA Self-Collection Kit (OGR-250, DNA Genonek). Libraries were processed according to Agilent SureSelect Target Enrichment System (Agilent Technologies, Santa Clara, Calif) for Illumina Paired-End Sequencing Library (Illumina, San Diego, Calif) using SureSelect Human All Exon V5 capture library (Agilent Technologies). Libraries were sequenced with 101 bp read length (HiSeq1500 sequencing platform, Illumina).

The read mapping, variant calling, and genome annotation were performed as described previously.[E1] On the basis of severe phenotype and the fact that the parents were asymptomatic, we hypothesized the condition to be caused by a mutation negatively affecting the coding sequence. We suspected the mutation to be either a de novo dominant change in the amino acid sequence or a homozygous or compound heterozygous recessive variant.

To find dominant variants, we filtered the data for coding mutations not present in control databases (The Exome Aggregation Consortium Browser, 1000 Genomes, NHLBI Exome variant server, and UK TWIN ALSPAC study cohorts as well as in-house databases). The remaining variants that showed phylogenetic conservation or were predicted damaging by bioinformatics tools (SIFT, Poly-Phen) were screened from the asymptomatic parents by Sanger sequencing. Because all these were present in at least 1 parent, we concluded that a de novo coding variant was unlikely to cause the disease.

For recessive variants, we filtered the data for rare homozygous or compound heterozygous coding variants (MAF < 0.001 in the aforementioned healthy control data sets). We identified recessive coding mutations in 10 genes. Only the compound heterozygous mutations in *HYOU1* gene were damaging and showed phylogenetic conservation. The candidate mutations were verified by capillary sequencing from blood DNA samples.

B- and T-cell immunophenotyping

Fresh EDTA-blood samples or PBMCs were used for B- and T-lymphocyte immunophenotyping, using 4- or 6-color flow cytometry panel with mAbs

against the surface antigens IgM, IgD, CD3, CD4, CD8, CD16/56, CD19, CD21, CD27, CD33, CD34, CD38, CD45, CD56, CD57, CD133, HLA-DR, CD62L, CD45RA, and CD45RO (BD Biosciences). The memory status of T cells was studied with the antibody panel including anti-CD45, anti-CD3, anti-CD4, anti-CD45RA, and anti-CCR7 (R&D Systems, Minneapolis, Minn).[E1]

Evaluation of T-cell responses is described in detail elsewhere.[E1] For the assessment of T-cell activation, fresh mononuclear cells were stimulated for 6 hours with anti-CD3, anti-CD28, and anti-CD49d (BD Biosciences). The cells were analyzed using a 4- or 6-color flow cytometry panel with mAbs against the antigens CD45, CD3, CD4, CD8, CD16, CD56, CD45, CD45RA, TCR-γ, CCR7, IFN-γ, and TNF.

Phenotyping of T_H17 and regulatory T cells

Phenotyping of IL-17–positive T_H17 cells and regulatory T (Treg) cells is described in detail elsewhere.[E1] To assess IL17 expression, fresh PBMNCs were stimulated for 16 hours with anti-CD3/anti-CD28 beads in the presence of Brefeldin A. Thereafter, the cells were fixed, permeabilized, and stained with anti-CD4, anti-CD69, and IL-17A (BD Biosciences) and analyzed with FACSAria II or FACSCanto II flow cytometer.

Treg cells were immunophenotyped from fresh blood with surface markers against CD4, CD25, and FOXP3 (BD Biosciences). For evaluation of Treg-cell suppressor capacity, $CD4^+CD25^+CD127^-$ Treg cells were sorted from whole blood using Human CD4+ T-Cell Enrichment Cocktail (Stemcell Technologies, Vancouver, British Columbia, Canada) and fluorescence-activated cell sorting with mAbs against CD4, CD25, and CD127 (BD Biosciences). The cells were incubated for 6 days with carboxyfluorescein succinimidyl ester (CFSE)-labeled autologous responder T cells in a ratio of 1:2. Anti-CD3/anti-CD28 beads (Life Technologies) were used as stimulus. $CD4^+$ cells were analyzed using FACSAria II flow cytometer (BD Biosciences). The suppression percentage was calculated with the following formula: 100 − [(% proliferation in presence of Treg cells/% proliferation in absence of Treg cells) × 100].

Monocyte and dendritic cell activation assays

For detailed immunophenotyping of monocytes and dendritic cells, immediately after collection, heparinized blood samples from the patient and 3 healthy controls were incubated in the presence of 100 ng/mL *Escherichia coli* LPS, 25 μg/mL polyinosinic-polycytidylic acid, or vehicle for 1 hour.

Stimulated samples were then mixed with surface marker antibodies (BDCA2 [Miltenyi Germany], CD1c [Miltenyi], CD14 [Invitrogen], CD19 [Invitrogen], CD80 [Becton Dickinson, Franklin Lakes, NJ], CD86 [Becton Dickinson], α4 [Serotec, Hercules, Calif], β7 [Becton Dickinson], CCR9 [R&D Systems], and CCR2 [R&D Systems]) or an equal concentration of their corresponding isotype controls and incubated for 20 minutes in the dark at room temperature. The red blood cells were then lysed by incubating the whole blood in 2 mL of FACS Lysing Solution (Becton Dickenson) for 10 minutes. The white blood cells were then pelleted out of solution by centrifugation (500*g* for 5 minutes, room temperature) and washed twice with a washing solution of 5% inactivated FCS (sterile, 0.22 μm filtered), 0.02% NaN3, and PBS. The washed cells were then fixed with 1% paraformaldehyde in PBS and stored overnight in the dark at +4°C. Staining controls for fluorescence compensation were prepared using 1 test volume of each specific antibody bound to OneComp Beads (eBiosceinces, Frankfurt, Germany). The data were analyzed with FACSCalibur flow cytometer (BD Biosciences).

Neutrophil functional studies

Neutrophil C5a and formyl-methionyl-leucyl-phenylalanine–induced chemotaxis was assessed according to standard clinical procedures. Neutrophil chemiluminescence test was performed according to standard protocols to assess reactive oxygen species generation.

To evaluate neutrophil activation, fresh blood was stimulated with 100 ng/mL *E coli* LPS for 1 hour, stained with surface marker antibodies (CD66b [Biolegend], CD14 [Invitrogen], CD66a [Diaclone], and CD11b [BD Biosciences]), as described above.

Fibroblast cultures and generation of inducible Flp-In 293 T-REx cell lines

Fresh skin biopsies were cut into small pieces and transferred to 12-well plates containing RPMI medium supplemented with 20% FBS, 1% L-glutamine, and 1% penicillin-streptomycin. The cells were grown for 2 to 3 weeks, then split onto 10-cm petri dishes, and frozen for later use when 80% confluent.

The cDNA constructs containing WT, p.Y231H, and p.A419P mutant *HYOU1* full-length coding sequences were commercially cloned into gateway compatible entry-vector (GenScript) and finally to pTO_HA_StrepIII_c_GW_FRT destination vector. Flp-In 293 T-Rex cells were transfected and cultured according to manufacturer's instructions (Life Technologies). The stable expression of mutant and WT Twin-Strep-tag HYOU1 upon tetracycline induction was confirmed by Western blotting and immunofluorescence microscopy (see Fig E1).

Western blotting and immunofluorescence microscopy

For Western blotting analysis, 5×10^5 Flp-In 293 T-Rex cells were seeded to 6-well plates, induced with tetracycline, harvested to Laemmli Sample Buffer, boiled, and ran to SDS-PAGE gel. Proteins were transferred onto nitrocellulose membrane and detected with anti-hemagglutin (HA) primary (HA-11, Covance) and horseradish peroxidase–conjugated secondary antibody. Signal was visualized by chemiluminescence. For immunofluorescent staining, cells were seeded onto coverslips, induced with tetracycline, fixed with 4% paraformaldehyde (PFA), and stained with anti-HA antibody and Alexa-488 goat antimouse IgG (Life Technologies, Thermo Fisher Scientific, Waltham, Mass). Nuclei were visualized with 4′-6-diamidino-2-phenylindole, dihydrochloride staining before mounting with Mowiol (Sigma, St Louis, Mo).

Affinity purification and mass spectrometry

Approximately 5×10^7 cells were lysed in HNN lysis buffer (50 mM HEPES, pH 8.0, 150 mM NaCl, 5 mM EDTA, 0.5% NP-40, 50 mM NaF, 1.5 mM Na3VO4, 1.0 mM phenylmethylsulfonyl fluoride, and 10 μL/mL protease inhibitor cocktail; Sigma). The proteins were bound using Strep-Tagtin sepharose and Bio-Spin chromatography column (Bio-Rad) and eluted with D-biotin (Thermo Scientific). Each sample was analyzed in quadruplicates: 2 biological replicates were analyzed in 2 technical replicates.

Mass spectrometry analyses were performed on an Orbitrap Elite ETD mass spectrometer (Thermo Scientific). Peak extraction and subsequent protein identification was achieved using Proteome Discoverer software (version 1.4.1.14, Thermo Scientific). Calibrated peak files were searched against the human component of UniProtKB/SwissProt database (www.uniprot.org) by a SEQUEST search engine. Error tolerances on the precursor and fragment ions were ±15 ppm and ±0.8 Da, respectively. Database searches were limited to fully-tryptic peptides with maximum 1 missed cleavage; carbamidomethyl cysteine and methionine oxidation were set as fixed and variable modifications, respectively. The biological clustering and pathway analysis was conducted using DAVID bioinformatics database (https://david.ncifcrf.gov).

Metabolomics profiling by mass spectrometry

Primary cultured skin fibroblasts from patient and 2 healthy controls were plated on 6-well plates and grown to 80% to 90% confluency. The cells were then trypsinised, washed twice with PBS, and then with deionized water for few seconds. Each cell line was analyzed in triplicate.

Approximately 10^6 cells per sample were taken for metabolomics analysis. Metabolites were extracted by adding 20 μL of labeled internal standard mix and 1 mL of cold extraction solvent (80/20 acetonitrile/H_2O + 1% formic

acid). Cells were then sonicated for 30 seconds, vortexed for 30 seconds, and incubated on ice for 10 minutes. After the centrifugation, supernatants were aspirated into eppendorf tubes. Metabolites were separated using Waters Acquity ultra performance liquid chromatography and analyzed by triple quadrupole mass spectrometry. One hundred metabolites from 16 different metabolite classes were analyzed. A detailed list of analyzed metabolites is available at https://www.fimm.fi/en/services/technology-centre/metabolomics/metabolomics-services . The enriched metabolic pathways were evaluated using quantitative enrichment analysis (http://www.metaboanalyst.ca).

Granulocyte isolation and electron microscopy

Plasma was separated from the blood cell fraction by centrifugation at 400*g* for 15 minutes. Plasma was removed and centrifuged at 1500*g* for 10 minutes at room temperature to pellet out the platelets. Platelet-poor plasma was collected. The cell fraction was carefully mixed with dextran (Sigma, Helsinki, Finland) and the erythrocytes were allowed to settle for 30 minutes at room temperature. The leukocyte fraction was collected, washed, resuspended in platelet-poor plasma, and carefully layered atop Ficoll (GE Life Sciences, Helsinki, Finland) and centrifuged at 700*g* for 15 minutes. After FICOLL gradient centrifugation, the PBMC layer was collected, the supernatant was removed, and the erythrocytes in the granulocyte fraction were lysed using a lysing buffer containing 1 mM EDTA, 150 mM NH4CL, and 10 mM $NaHCO_3$ in water for 3 minutes followed by centrifugation at 483*g* for 8 minutes at room temperature. Cells were washed twice using 0.9% NaCl. Cells were then resuspended in HBSS (Thermo Scientific) medium until use. Trypan blue exclusion assay was used to assess the viability of the isolated granulocytes.

Approximately 10^6 granulocytes from patient and 2 healthy controls were fixed with 2-fold strength fixative in 1:1 ratio to give final concentration of 2.5% glutaraldehyde (Sigma) in 0.1 mol natrium cacodylate buffer, pH 7.4. After 2 hours of fixation, the cells were processed for transmission electron microscopy by osmication, dehydration in a graded ethanol series and acetone, and infiltration gradually with Epon at room temperature. Thin sections were imaged by transmission electron microscope (Tecnai F12; FEI Comp.) operated at 80 kV. The images were acquired at nominal magnification of 4800× using Orius SC 1000B CCD camera (Gatan Inc, Pleasanton, Calif). The sampling for target cells was randomized, provided that the cells had at least 2 disguised nuclear profiles.

For estimation of the size and frequency of mitochondria from control and patient granulocytes, mitochondria and cytoplasmic area were manually traced in the digital images and measured using Image-Pro Analyzer 7.0 (Media Cybernetics Inc, Rockville, Md). The total cytoplasmic areas calculated were 670, 530, and 560 μm^2 for 2 control specimens and patient, respectively.

RNA sequencing

For RNA sequencing, cultured primary fibroblasts from the studied patient and 2 healthy controls were plated in 6-well plates at 15,000 cells/well. The following day, the cells were mock-treated or Tunikamycin-stimulated (1 ng/μL) for 1 hour. The RNA was extracted with Qiagen All-Prep kit (Qiagen). All samples were studied in biological triplicates and technical replicates.

Published STRT protocol[E2] was applied using 10 ng total RNA as template and following minor modifications. Forty-eight barcodes were used (see Table E2); the cell capture buffer contained 0.1% Triton X-100, 800 nM T30-VN-oligo, 2 mM deoxynucleotide (dNTP) mix, and 2 μM template-switching oligonucleotide (TSO) without magnesium chloride. After cDNA synthesis, all 48 cDNAs were pooled into one 2-mL tube using 10% PEG-6000 and 0.9 mol NaCl (final concentration). The purified cDNA was first amplified using 14 cycles of PCR and later an additional 10 cycles to introduce a complete set of adapters for Illumina single read sequencing. Ready library was size-selected using sequential AMPure XP bead selection protocol where 0.7× and 0.22× bead/PCR product ratios were used.

After the sequencing, the reads were processed by STRTprep package (https://github.com/shka/STRTprep; manuscript in preparation). Low-quality reads and PCR duplicons were excluded from the analysis. The reads were trimmed and separated by the barcodes[E3] and aligned to GRCh37/hg19 genome, human ribosomal DNA unit (GenBank: U13369) using TopHat.[E4] The expression levels were estimated by strand-specific 50-bp windows (sliding 25 bp). ERCC spike-in RNA read counts, spike-in 5'-end capture rate, endogenous polyA+ RNA rate, and PC1 and PC2 scores in Principal component analysis (PCA) plot were used for sample quality assessment.

For differential expression tests, we selected 2 deeply sequenced biological replicates in each comparing group, and 1 technical replica in each biological replica was used. Then, the fluctuated regions, which had broader coefficients of variation rather than technical variation of spike-in RNA, were selected ($P < .1$ with Bonferroni correction; unpublished data). Finally, the significance of differential expression in the fluctuated regions was assessed by SAMstrt package.[E5] Genes with reads mapping to protein-coding RNA sequence with Q value of less than 0.1 and P value of less than .1 were considered differentially expressed. The biological clustering and pathway analysis was conducted using DAVID bioinformatics database.

Evaluation of mitochondrial respiratory capacity

The XF Mito Stress Test Kit (Seahorse Bioscience, North Billerica, Mass) was used to evaluate the basal and maximal mitochondrial respiration and the cellular ATP production. The patient and healthy control (n = 3) primary skin fibroblasts were seeded to XF cell culture microplates at a density of 30,000 cells/well (12 technical replicates per case) and incubated overnight at 37°C in normal medium (RPMI supplemented with 20% FBS, 1% L-glutamine, and 1% Penicillin-Streptomycin). The next day, the media was replaced with assay medium (XF base medium supplemented with 5 mM pyruvate, 5 mM glutamine, and 10 mM glucose) and cells incubated in a non-CO_2 incubator for 1 hour at 37°C. The plate was then loaded into the XF^{e}96 Extracellular Flux Analyzer (Seahorse Bioscience) and measurements were carried out according to the XF Mito Stress Test Kit protocol. The resulting data were analyzed with the XF Analyzer/Wave software (Seahorse Bioscience).

REFERENCES

E1. Haapaniemi EM, Kaustio M, Rajala HL, van Adrichem AJ, Kainulainen L, Glumoff V, et al. Autoimmunity, hypogammaglobulinemia, lymphoproliferation and mycobacterial disease in patients with dominant activating mutations in STAT3. Blood 2015;125:639-48.

E2. Islam S, Zeisel A, Joost S, La Manno G, Zajac P, Kasper M, et al. Quantitative single-cell RNA-seq with unique molecular identifiers. Nat Methods 2014;11:163-6.

E3. Kivioja T, Vaharautio A, Karlsson K, Bonke M, Enge M, Linnarsson S, et al. Counting absolute numbers of molecules using unique molecular identifiers. Nat Methods 2012;9:72-4.

E4. Trapnell C, Pachter L, Salzberg SL. TopHat: discovering splice junctions with RNA-Seq. Bioinformatics 2009;25:1105-11.

E5. Katayama S, Tohonen V, Linnarsson S, Kere J. SAMstrt: statistical test for differential expression in single-cell transcriptome with spike-in normalization. Bioinformatics 2013;29:2943-5.

E6. Hauck F, Klein C. Pathogenic mechanisms and clinical implications of congenital neutropenia syndromes. Curr Opin Allergy Clin Immunol 2013;13:596-606.

E7. Boztug K, Jarvinen PM, Salzer E, Racek T, Monch S, Garncarz W, et al. JAGN1 deficiency causes aberrant myeloid cell homeostasis and congenital neutropenia. Nat Genet 2014;46:1021-7.

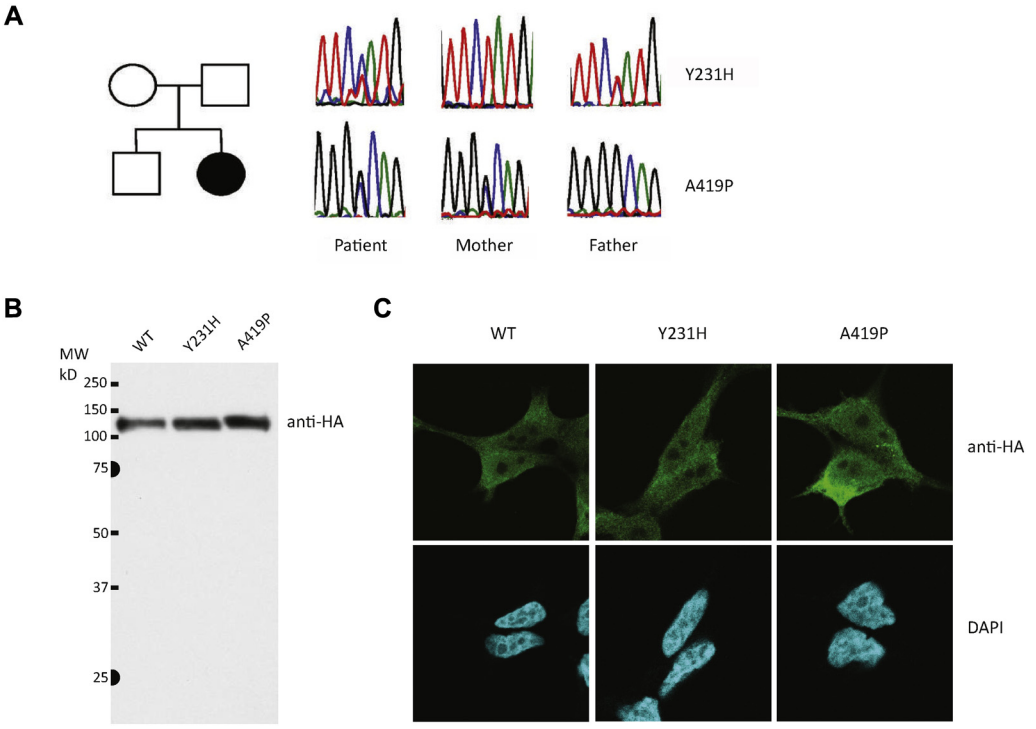

FIG E1. A, Sanger sequencing of the HYOU1 mutants in index patient and her parents. **B,** HYOU1 protein expression and subcellular localization **(C)** in Flp-In 293 T-REx cells. Both mutants are expressed equally, and the subcellular localization is unaltered. *DAPI*, 4′-6-diamidino-2-phenylindole, dihydrochloride; *HA*, Hemaggluting tag.

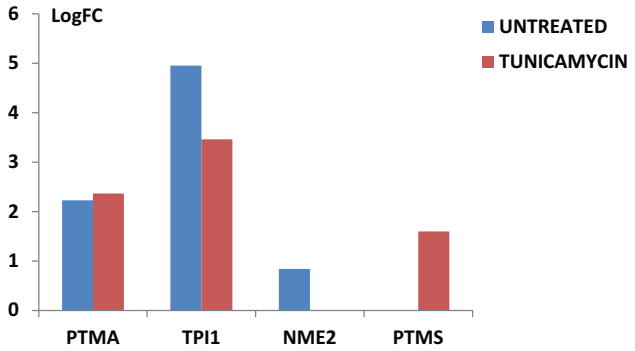

FIG E2. Some of the ectopic interaction partners of the mutant HYOU1 proteins were upregulated on the RNA sequencing of patient primary fibroblasts. Genes with statistically significant differential expression ($P < .05$) are shown. *NME2*, Nucleoside diphosphate kinase B; *PTMA*, prothymosin alpha; *PTMS*, parathymosin; *TPI1*, triosephosphate isomerase 1.

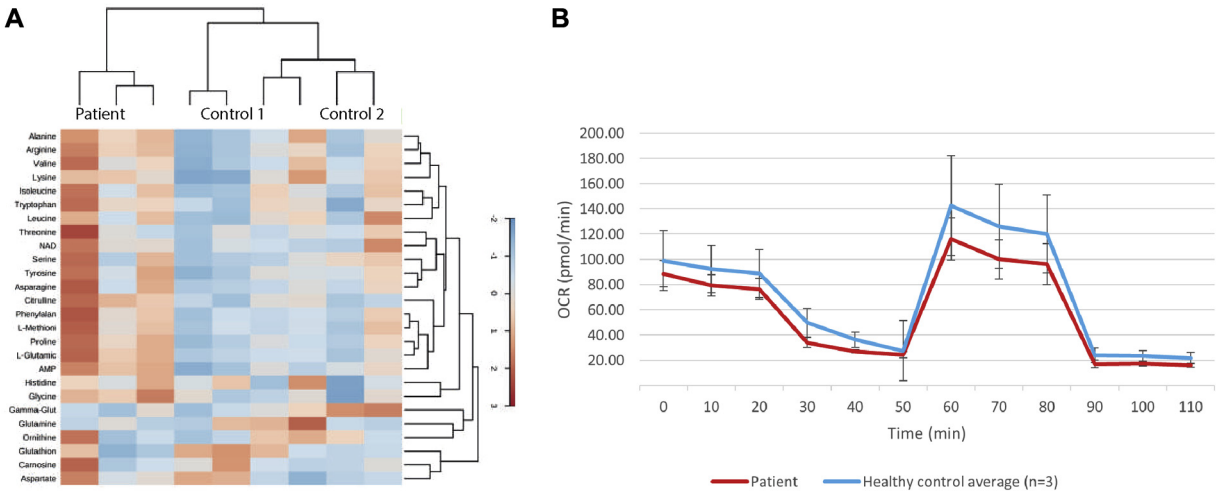

FIG E3. A, Significantly altered metabolites in primary fibroblasts. **B,** Mitochondrial respiration capacity on patient and healthy control primary fibroblasts. The patient cells perform on low normal range, but no statistically significant abnormality is evident. Time points between 0 and 20 minutes evaluate basal mitochondrial respiration, 20 to 50 minutes cellular ATP production, and 50 to 80 minutes the maximal respiratory capacity. *OCR*, Oxygen consumption rate.

TABLE E1. Immunological features of the patient

Immunologic feature		Normal range/ healthy control median value	Patient
Leukocytes		3,400-8,200	3500
	Lymphocytes	1,000-4,500	910 ↓
	Monocytes	200-800	350
	Neutrophils	1,500-7,500	150-4000 ↓
	Basophils	0-100	0-10 ↓
	Eosinophils	100-400	0 ↓
	Platelets	150,000-360,000	342000
	NK cells ($CD3^-CD16^+/56^+$)	90-600	306
Dendritic cells			
Plasmacytoid	$lin^-HLA\text{-}DR^+CD123^+CD11c^-$	0.1%-0.3%	0.05% ↓
Monocytoid	$lin^-HLA\text{-}DR^+CD123^-CD11c^+$	0.1%-0.3%	0.02% ↓
$CD3^+$ T cells		700-2,100 (71%)	694 (78%)
	$TCR\alpha\beta^+$	0.94	1
	$TCR\gamma\delta^+$	0.06	<0.1%
	$CD4^-CD8^-$ $TCR\alpha\beta^+$	<1%	2.5% ↑
$CD3^+CD4^+$ T cells		458-1,400 (51%)	454 (66%)
	$CD45RO^+$	51%	—
	$CD45RA^+$	47%	82.8% ↑
TCM	$CCR7^+CD45RA^-$	38%	12.5% ↓
Naive	$CCR7^+CD45RA^+$	45%	74.7% ↑
TEM	$CCR7^-CD45RA^-$	11%	6.7%
Temra	$CCR7^-CD45RA^+$	4%	3.1%
	Granzyme B^+	1%	1%
Unstimulated	IFN-γ/TNF-α secretion	0%	0.7%
Stimulated*	IFN-γ/TNF-α secretion	5%	7.7%
Treg cell	$FOXP3^+CD25^+$	2.3%-7.8%	0.23% ↓
	Suppressive capacity		Normal
T_H17	$CD69^+IL17^+$		1.41%
$CD3^+CD8^+$ T cells		200-1200	243 (33%)
	$CD45RO^+$	41%	—
	$CD45RA^+$	72%	95.3% ↑
TCM	$CCR7^+CD45RA^-$	8%	0.6% ↓
Naive	$CCR7^+CD45RA^+$	35%	72% ↑
TEM	$CCR7^-CD45RA^-$	27%	2.9% ↓
Temra	$CCR7^-CD45RA^+$	33%	24.3% ↓
	Granzyme B^+	11%	12.5%
Unstimulated	IFN-γ/TNF-α secretion	0%	1.2% ↑
Stimulated*	IFN-γ/TNF-α secretion	7.20%	7.6%
$CD19^+$ B cells†		70-230	8 ↓
Transitional	$CD38^{hi}IgM^{hi}$	0.6%-3.5%	0%
Naive	$CD27^-IgD^+$	—	10%
Mature B cells	$CD21^+$	11%-45%	94% ↑
Memory	$CD27^+$	15%-45%	73% ↑
Marginal zone-like	$CD27^+IgD^+IgM^+$	7.2%-30.8%	57%
Switched memory	$CD27^+IgD^-IgM^-$	6.5%-29.2%	0.04% ↓
Plasmablasts	$CD38^{++}IgM^-$	—	0
Activated	$CD38^{low}CD21^{low}$	0.6%-3.5%	7%
Immunoglobulins (prior IVIG)†			
	IgG	6.8-15.0 g/L	8.0
	IgA	0.52-4.02 g/L	2.79
	IgM	0.47-2.84 g/L	1.69
	IgE	0-110 IU/L	13
Neutrophil C5a and FMLP-induced chemotaxis			Severely reduced
Neutrophil CD11b expression after stimulation (% of normal)			87%
Neutrophil ROS generation (% of normal)			170% ↑
Neutrophil CD66a expression		19.6%	146% ↑
Neutrophil CD66a expression after LPS stimulation		55.5%	90.6% ↑
Complement	Classical, Alternative, MBL		Normal

(Continued)

TABLE E1. *(Continued)*

Immunologic feature	Normal range/ healthy control median value	Patient
Lymphocyte proliferative responses to mitogens	PHA, concanavalin A, tuberculin (PPD), pokeweed mitogen	PHA weak, concanavalin A weak, PPD weak, pokeweed mitogen normal
Specific antibodies against vaccine antigens	Antitetanus, antidiphtheria, antipneumococcal polysaccharide	Tetanus weak, Pneumococcal undetectable

$CD3^+$ T-cell, $CD4^+$ cell, $CD8^+$ cell, and $CD19^+$ cell numbers are indicated as absolute counts (cells/mm^3) and relative percentages of parent population (%). Control values are indicated either as absolute count ranges or as medians from 3 healthy controls (%).

FMLP, Formyl-methionyl-leucyl-phenylalanine; *IVIG*, intravenous immunoglobulin therapy; *MBL*, Mannan-binding lectin pathway; *NK*, natural killer; *PPD*, purified protein derivative; *ROS*, reactive oxygen species; *TCM*, central memory T cell; *TEM*, effector memory T cell; *Temra*, effector memory RA T cell.

*Stimulated with anti-CD3, anti-CD28.

†Data obtained before rituximab therapy.

TABLE E2. Analysis of monocyte and dendritic cell activation (fluorescence intensity shown as arbitrary units)

Mitogen (dilutions)	% of control
PHA (1:50, 1:200, 1:500)	23%, 36%, 32%
Concanavalin A (1:50, 1:200, 1:500)	24%, 66%, 17%
Pokeweed mitogen (1:100)	82%
Tuberculin purified protein derivative (PPD)	0%

TABLE E3. Lymphocyte proliferative responses to mitogens

		lin$^-$HLA-DR$^+$CD123$^+$ dendritic cells		$CD14^+$ monocytes	
Marker		**Healthy control median (n = 3)**	**Patient**	**Healthy control median (n = 3)**	**Patient**
	$CD86^+$	15	7.47 ↓	19.8	8.32 ↓
LPS+	$CD86^+$	27.1	19.6	42.9	14.6 ↓
PolyI:c	$CD86^+$	7.08	NA	27.8	NA
	$CD80^+$	6.29	7.66	12.8	13.6
LPS+	$CD80^+$	7.61	10.6	27.1	21.9
PolyI:c	$CD80^+$	12.8	NA	6.85	NA
	$\alpha4^+$	451	614	160	42.9 ↓
LPS+	$\alpha4^+$	310	703	209	50.5 ↓
PolyI:c	$\alpha4^+$	121	NA	106	43.5 ↓
	$\beta7^+$	167	218	114	24.2 ↓
LPS+	$\beta7^+$	131	211	148	37.6 ↓
PolyI:c	$\beta7^+$	60	26.3	64.4	17.2 ↓
	$CCR9^+$	77.1	10.6 ↓	61.8	38.5 ↓
LPS+	$CCR9^+$	158	10.1 ↓	98.9	48 ↓
PolyI:c	$CCR9^+$	14.55	12.1	68.6	38.8 ↓
	$CCR2^+$	27.7	45.4 ↑	81.3	80.3
LPS+	$CCR2^+$	33.5	58.5 ↑	97.8	79.9
PolyI:c	$CCR2^+$	32.8	29	69.05	81.7

NA, Not applicable/available.

TABLE E4. Genetic causes of congenital neutropenia*

Gene	*ELANE*	*HAX1*	*VPS45*	*JAGN1*	*G6P3*	*HYOU1*	*LAMTOR2*	*AP3B1*	*RAB27A*
Clinical characteristics									
Inheritance	AR, AD	AR	AR	AR	AR	*AR*	AR	AR	AR
Infection susceptibility	Bacteria	Bacteria	Bacteria	Bacteria	Bacteria	*Bacteria, herpesvirus*	Bacteria	Bacteria	Bacteria
Immunology	Neutropenia, cyclic neutropenia	Neutropenia	Neutropenia, hypergammaglobulinemia, myelofibrosis	Neutropenia	Neutropenia, thrombocytopenia	*Granulocytopenia, thrombocytopenia, anemia, B-cell deficiency, dendritic cell deficiency*	Neutropenia, hypogammaglobulinemia	Granulocytopenia, coagulation defects, decreased NK and T-cell cytotoxicity	Neutropenia, decreased NK and T-cell cytotoxicity
Other features	—	Neurological impairment (some cases)	Hepato-, spleno-, & nephromegaly (extramedullary hematopoiesis)	Bone and dental anomalies	Syndromic patients	*Hypoglycemia, mild bone anomalies*	Oculocutaneous albinism	Oculocutaneous albinism	Oculocutaneous albinism
Malignancy predisposition	+	+	+	−	−	−	−	−	−
Molecular pathogenesis									
Cellular compartment	ER	Mitochondria	ER, vesicular system	ER	ER	*ER, mitochondria*	Vesicular transport system	Vesicular transport system	Vesicular transport system
Pathogenic mechanism	ELANE accumulation in the ER, UPR induction, & neutrophil apoptosis	Mitochondrial destabilization, disturbed stress signaling -> neutrophil apoptosis	Defective endosomal trafficking	Protein accumulation in the ER, defective glycosylation, UPR induction -> neutrophil apoptosis	Impaired ER glucose metabolism and protein glycosylation -> UPR & neutrophil apoptosis	*Altered UPR and redox balance*	Impaired vesicular transport	Impaired vesicular transport	Impaired vesicular transport

The clinical and molecular characteristics of HYOU1 deficiency have been italicized and underlined.
AR, Autosomal recessive; *AD*, autosomal dominant; *ER*, endoplasmic reticulum; *UPR*, unfolded protein response.
*Genes with function in cell stress pathways or in the endolysosomal system are shown.[E6,E7]